



ELSEVIER



CrossMark

Available online at www.sciencedirect.com

ScienceDirect

Proceedings of the Combustion Institute 35 (2015) 1693–1700

**Proceedings
of the
Combustion
Institute**

www.elsevier.com/locate/proci

n-Butanol droplet combustion: Numerical modeling and reduced gravity experiments

Fahd E. Alam^a, Y.C. Liu^{b,1}, C.T. Avedisian^b, F.L. Dryer^c,
T.I. Farouk^{a,*}

^a Department of Mechanical Engineering, University of South Carolina, Columbia, SC 29208, USA

^b Sibley School of Mechanical and Aerospace Engineering, Cornell University, Ithaca, NY 14853, USA

^c Department of Mechanical and Aerospace Engineering, Princeton University, Princeton, NJ 08544, USA

Available online 16 July 2014

Abstract

Recent interest in alternative and bio-derived fuels has emphasized butanol over ethanol as a result of its higher energy density, lower vapor pressure and more favorable gasoline blending properties. Numerous efforts have examined the combustion of butanol from the perspective of low dimensional gas-phase transport configurations that facilitate modeling and validation of combustion kinetics. However, fewer studies have focused on multiphase butanol combustion, and none have appeared on isolated droplet combustion that couples experiments with robust modeling of the droplet burning process. This paper presents such an experimental/numerical modeling study of isolated droplet burning characteristics of *n*-butanol. The experiments are conducted in an environment that simplifies the transport process to one that is nearly one-dimensional as promoted by burning in a reduced gravity environment. Measurements of the evolution of droplet diameter ($D_o = 0.56\text{--}0.57$ mm), flame standoff ratio ($FSR \equiv D_f/D$) and burning rate (K) are made in the standard atmosphere under reduced gravity and the data are compared against numerical simulation. The detailed model is based on a comprehensive time-dependent, spherically-symmetric droplet combustion simulation that includes spectrally resolved radiative heat transfer, multi-component diffusive transport, full thermal property variations and detailed chemical kinetic. The simulations are carried out using both a large order kinetic mechanism (284 species, 1892 reactions) and a reduced order mechanism (44 species, 177 reactions). The results show that the predicted burning history and flame standoff ratios are in good agreement with the measurements for both the large and reduced order mechanisms. Additional simulations are conducted for varying oxygen concentration to determine the limiting oxygen index and to elucidate the kinetic processes that dictate the extinction of the flame at these low oxygen concentrations. © 2014 The Combustion Institute. Published by Elsevier Inc. All rights reserved.

Keywords: *n*-Butanol; Biofuel; Droplet combustion; Microgravity; Modeling

* Corresponding author. Fax: +1 803 777 0106.

E-mail address: tfarouk@sc.edu (T.I. Farouk).

¹ Current Address: Department of Computer Science, Engineering Science and Physics, University of Michigan-Flint, Flint, MI 48502, USA.

1. Introduction

The growing interest in normal butanol (*n*-C₄H₉OH, boiling point of 391 K) as a non-petroleum fuel for internal combustion engines,

either as a gasoline surrogate or an additive to increase performance of both gasoline and diesel fuels due to its favorable properties relative to ethanol [1–3], has stimulated fundamental research to understand its combustion kinetics. The experimental configurations used for this purpose typically incorporate a zero or one-dimensional transport dynamic (i.e., in shock tubes [4–6]), constant volume combustion chambers [7], jet stirred reactors [8–14], and opposed flow diffusion flames [15] with pre-vaporized butanol to facilitate *ab initio* modeling of the flow and combustion dynamics involved.

Few studies of *n*-butanol combustion have been carried out to evaluate kinetic mechanisms derived from spray or droplet dynamics, and none have done so incorporating detailed kinetic scheme. The work of Wang et al. [16] is noteworthy for using the environment of a direct injection diesel engine fueled with a mixture of diesel fuel and *n*-butanol to validate a reduced kinetic mechanism using the KIVA-3vr2 code [17], which requires certain spray model constants to be calibrated and adjusted to make the liquid and vapor penetrations match experimental measurement of these quantities, as well as submodel inputs for turbulence, gas jet/collision for spray, spray/droplet breakup, and droplet evaporation and wall collision dynamics.

The simplest configuration for a liquid fuel that is amenable to detailed simulation is an isolated droplet burning in an environment in which streamlines of the flow are radial and the mass and energy transport are one-dimensional due entirely to the evaporation process. As simple as the one-dimensional droplet flame may appear, it is relevant to the complex environment of a spray through elements that carry over to the spray environment [18]. These include moving boundary effects, unsteady heat conduction and mass diffusion in the droplet and surrounding gas, variable properties (dependent on temperature and composition), phase equilibrium at the interface, radiation dynamics, and a detailed kinetic mechanism for the combustion process. Computer simulations based on assuming spherical symmetry recently been applied to a range of alkane, alcohol and methyl ester systems [19–22].

In this paper we present a comprehensive numerical simulation of the combustion of isolated *n*-butanol droplets that assumes spherical symmetry. The intent is to examine the potential of the combustion kinetics previously developed for butanol using targets from low dimensional gaseous configurations as noted previously, to predict droplet combustion targets. These include the evolutions of droplet and flame diameters (D and D_f , respectively), and the burning rate $K \left(\equiv \left| \frac{dD^2}{dt} \right| \right)$. The initial droplet diameters (D_0) are essentially constant in this study (between

0.56 mm and 0.57 mm) and the combustion process is examined in the standard atmosphere. The simulations presented here employ a detailed kinetic mechanism for *n*-butanol that incorporates 284 species and 1892 reactions [23]. The results are compared to experimental data as well as to predictions that employed a reduced order kinetic model [16] consisting of 44 species and 177 reactions.

2. Experimental setup and procedure

Individual *n*-butanol droplets are formed, deployed, and ignited under conditions that achieve nearly spherically symmetric burning. As with a number of prior studies (e.g., [22,24,25]) nearly spherical flames were achieved by burning the test droplets under free-fall conditions. Figure 1 illustrates the experimental procedures for the present study.

A piezoelectric droplet generator [26] propels fuel droplets (D_0 on the order of between 0.5 mm and 0.6 mm) onto the intersection of two $14 \mu\text{m}$ SiC fibers crossed at approximately 60° [25,27]. The fuel droplet is then ignited

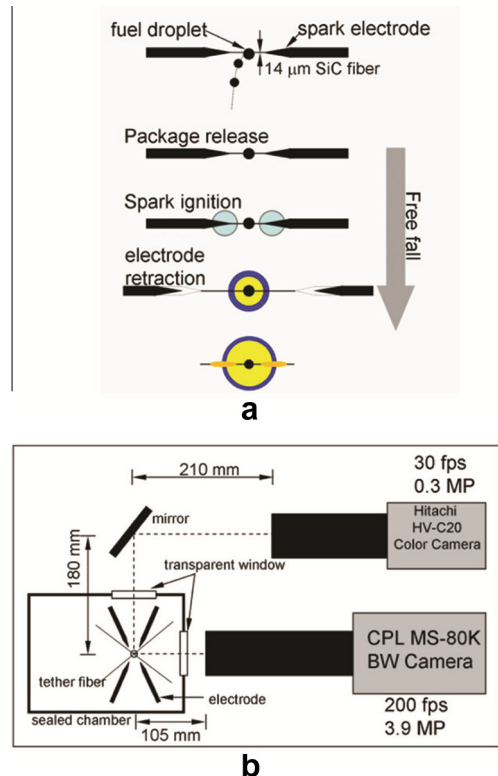


Fig. 1. (a) Schematic diagram of experimental procedure to deploy droplets onto SiC fiber. (b) Experimental setup (numbers in millimeters not to scale).

320 ms after the initiation of free-fall by symmetric spark discharge across two electrode pairs positioned on opposite sides of the droplet. The sparks remain activated for about 800 μs (or $\sim 1\%$ of the nominal 0.63 s burning time of the droplets examined in this study) and then the electrodes are rapidly retracted away from the combustion zone after burning commences.

Since a test droplet is anchored by fibers while it burns in the current investigation, the potential for an influence of the supporting fiber on burning was examined by comparing free-floating and fiber-supported burning histories of droplets with nominally the same initial diameters. The evolutions of D and D_f for free and supported droplets were found to be well correlated [27,28].

Video imaging is the main diagnostic that provides a record of the burning history from which quantitative measurements are extracted. The droplet burning process is simultaneously recorded by individual cameras from two orthogonal views (Fig. 1b). A color video camera (Hitachi HV-C20 (0.3 MP per frame) operated at 30 fps with a Nikkor 135 mm f/2.0 lens and two Kenko 36 mm extension tubes) documented self-illuminated flame images. A high-speed high-resolution black and white (BW) digital camera (3.9 MP per frame Canadian Photonics Labs (CPL), Inc. MS-80K, operated at 200 fps, and fitted with an Olympus Zuiko 90 mm f/2.0 lens, an Olympus OM Telescopic Extension Tube 65–116 mm (fixed at 100 mm), and a Vivitar MC 2X teleconverter) recorded the backlit droplet images during the burn. Backlighting was provided by a 1-Watt LED lamp (Black Diamond Equip, LTD). Three separate repetitions having identical initial conditions were performed to examine experimental repeatability.

Quantitative data were obtained from the BW digital video records of the droplet burning histories through a frame-by-frame analysis using a MATLAB-based algorithm [29], which was periodically cross-checked with manual measurements using Image-Pro Plus v6.3. Flame diameters are determined from the color images using CorelDraw 9, in which a digital ellipse is manually positioned around the outer luminous zone of the flame to yield an equivalent flame diameter.

3. Numerical modeling

The experimental results are compared against predictions using a previously developed numerical model of spherically symmetric droplet combustion that is described in detail elsewhere [20–22]. The model features detailed gas phase kinetics, here being for *n*-butanol, spectrally resolved radiative heat transfer, multi-component transport and heat transfer perturbations due to the presence of the tether fibers. The data

correlations of Daubert and Danner [30] were used to calculate the liquid phase properties of *n*-butanol.

The simulations were conducted using the detailed and reduced kinetic models of Sarathy et al. [23] and Wang et al. [16], respectively. It should be noted that the detailed models employed in this simulation are strictly valid for high temperature oxidation and do not contain any of the low-intermediate temperature reaction pathways. Experimental studies of gas phase *n*-butanol oxidation processes exhibit low and intermediate temperature kinetic behavior only at high pressure [31]. Typical simulations with 350 grid points on a stand-alone eight core linux workstation having 2.4 GHz processor speed and 20 GB RAM employing the detailed kinetic model took ~ 68 CPU hours, were as the calculations with the reduced model were completed in ~ 0.34 CPU hours. Additionally, we note that we also tried to use the kinetic model of Harper et al. [32] but were unable to obtain any converged solutions.

In the simulations, the Dirichlet condition of fixed ambient composition (fixed O_2 and N_2 composition) and temperature (298 K) are imposed on the far-field. A trapezoidal initial temperature profile having a peak temperature of 2000 K and ignition energy of 0.06 J was used to simulate the spark ignition source of the experiments [22]. The ignition energy is prescribed by the energy density ($\rho C_p \Delta T$) of the initially specified temperature profile integrated over the trapezoidal-shaped region.

The results of the simulations are compared with the experimental data in the next section, and then used to simulate additional conditions to provide insights into the *n*-butanol droplet burning process.

4. Results and discussions

Figure 2 shows an exemplar set of photographs of the *n*-butanol droplet burning history as obtained from the digital video records. Some

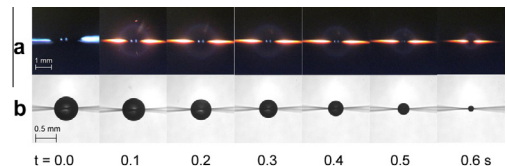


Fig. 2. (a) Selection of color images of droplet showing flame structure (glow is due to flame/fiber interaction). (b) Selection of BW images for a burning *n*-butanol droplet in atmospheric air. (For interpretation of the references to colour in this figure legend, the reader is referred to the web version of this article.)

initial asymmetry of the flame structure exists due to gas motions induced by spark ignition and electrode retractions, though the flame shapes were largely spherical throughout the burning process. As is evident from Fig. 2, no soot formation is observed for *n*-butanol droplet combustion (i.e., no soot shell). The sequences of color images show a faint blue luminosity indicative of CH emissions, and no luminosity characteristic of soot formation.

Figure 3 illustrates the quantitative measurements of the evolution of droplet diameter and FSR of three individual experimental runs in the coordinates of the classical D^2 law [33] with nominally the same initial diameters. Both the figures indicate that the experiments are highly repeatable with little scattering in the data, especially for the droplet diameter. It is apparent from the droplet diameter regression that no extinction is observed.

The evolution of flame diameter as extracted from the color images is shown in Fig. 3b, presented in term of relative position of the flame boundary to the droplet boundary, FSR. The trends are significantly different from the classical theory that predicts D_f/D to be constant [33]. Due to the lower resolution of the color camera and

greater difficulty of identifying the flame boundary (taken as the outer luminous zone as discerned manually), there are fewer flame diameter data, and with larger uncertainty, compared to the droplet diameter measurements (Fig. 3a).

Figure 4 compares the simulated evolution of droplet diameter and FSR against experimental values for both detailed and reduced kinetic schemes. Predictions from both the detailed and reduced model are also summarized. The standard deviations pertaining to each averaged data point are calculated from the data for the three individual experiments. The predicted droplet diameter regressions from both the models show good qualitative trends in comparison to the experimental data. Up to approximately 50% of the burn, predictions from the model are almost identical and are in very good agreement with the measured data. However, beyond 50% of the burn-time slight deviation between the predictions and measurements start to exist. The discrepancy with the measurements increases when the reduced kinetic mechanism is employed compared to the detailed kinetic model, as expected since reduced kinetic models removed possibly finer kinetic aspects during the process of reduction. However, the variation between the two models for the droplet diameter regression is not significant. Overall increase in deviation for the predicted and experimental values during the latter stages of burning (i.e. with smaller droplet diameter, viz at smaller Damköhler numbers) may be attributed to droplet-fiber interactions or possibly a limitation of the combustion kinetics.

The evolution of predicted peak gas temperature (T_{\max}) is also shown in Fig. 4 with the temporal scale (i.e. t/D_0^2) being presented in logarithmic format to provide more detailed insight into the

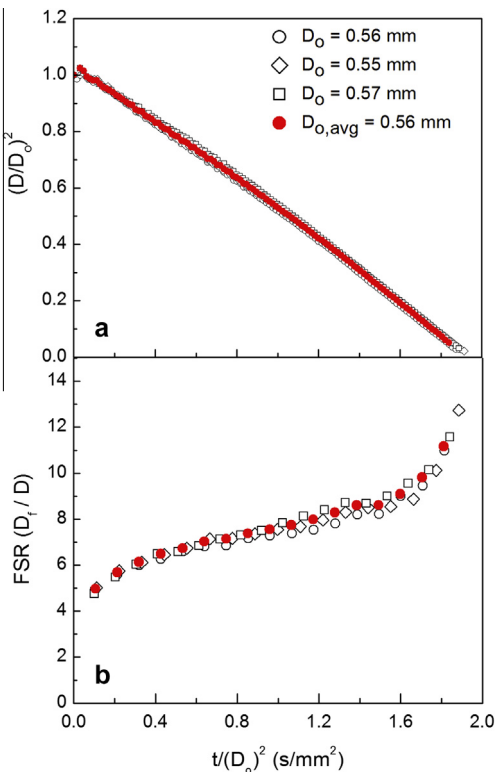


Fig. 3. Evolution of *n*-butanol droplet (a) burning history (b) flame stand-off ratio for three individual runs (1 atm, 21% O_2 /balance N_2).

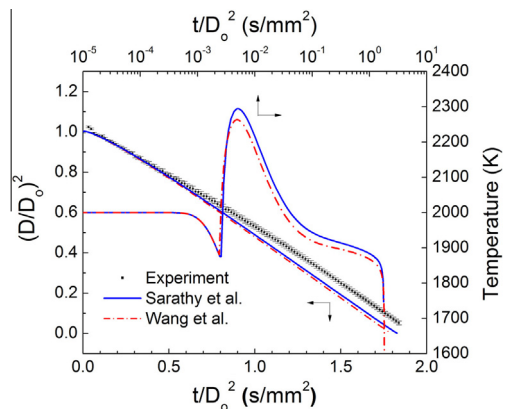


Fig. 4. Predicted evolution of droplet diameter and peak temperature profiles for *n*-butanol droplet ($D_0 = 0.56$ mm, 1 atm, 21% O_2 /balance N_2). The secondary axes (upper logarithmic and right hand) correspond to temperature evolution.

earlier transient evolution of T_{max} . It can be seen that there are negligible differences between the two kinetic mechanisms in the T_{max} , and the ignition delay time between both models is indistinguishable with heating rates (i.e. dT_{max}/dt) being virtually identical. The peak temperature decreases before ignition resulting from the endothermic reactions, which is also almost identical for the two models.

The difference in peak temperature predicted by the two kinetic models are ~ 40 K and ~ 30 K during maximum temperature difference and quasi-steady condition, respectively. The variation in the peak gas temperature is due to the additional reaction pathways that are considered in the detailed model. Due to these additional reaction pathways, the net of endothermic and exothermic reaction processes lead to a higher sensible enthalpy within the flame zone. It is interesting to note that even though the reduced model predicts lower flame temperature during the quasi-steady burn, K_{avg} is slightly higher.

Figure 5 compares predicted droplet burning of *n*-butanol droplet burning against two other prominent oxygenated fuels (methanol & ethanol)

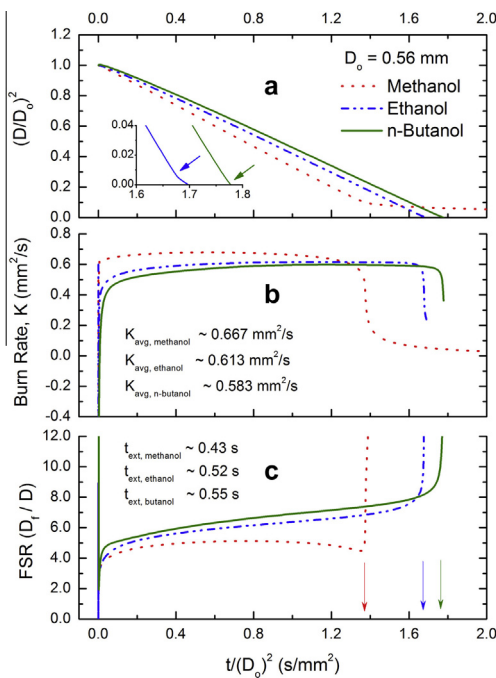


Fig. 5. Numerical prediction comparison for methanol, ethanol and *n*-butanol droplet combustion: (a) burning history with an enlarged view of ethanol & *n*-butanol burning prior to extinction (blue arrow: ethanol slope change indicator, green arrow: *n*-butanol full depletion indicator), (b) burning rate, (c) FSR. $D_0 = 0.56$ mm, 21% O_2 /balance N_2 , 1 atm. (For interpretation of the references to colour in this figure legend, the reader is referred to the web version of this article.)

under same initial diameters, ambient and ignition conditions is shown in Fig. 5. *n*-butanol is found to have the slowest average burning rate [$K_{C_4H_9OH}$ (0.583 mm^2/s) < $K_{C_2H_5OH}$ (0.613 mm^2/s) < K_{CH_3OH} (0.667 mm^2/s)] (Fig. 5a). In addition, as droplet burning proceeds both methanol and ethanol undergo extinction at finite diameters mainly due to a water dissolution effect whereas *n*-butanol burns to completion. In general, the average burning rates (K_{avg}) for the detailed model predictions were found to be slightly lower in comparison to the reduced model. The burning rate computed from the detailed and reduced reaction mechanisms differed by $\sim 3\%$: 0.583 mm^2/s for the detailed mechanism and 0.602 mm^2/s for the reduced mechanism. Both kinetic models predict complete burning without any flame extinction, as also observed experimentally. It is also observed that among the three oxygenated fuels, *n*-butanol extinguished latest compared to other two.

Figure 6 compares predicted and measured FSR data averaged over the three individual experimental runs where the numerically computed flame position was based on the location of T_{max} [20] and the location of maximum heat release rate (HRR_{max}). Error bars are indicated (mean and standard deviation). The results from both kinetic models capture the qualitative trends of the experiments quite well. The analysis indicates that the HRR_{max} option is more favorable compared to T_{max} in predicting the flame location. The FSR of *n*-butanol increases throughout the droplet lifetime due to thermal buffering of the far field that leads to decreased loss of heat from the flame structure and an ever increasing FSR as burning progresses. The thermal buffering of the far field is typically observed for sub-millimeter sized droplets. Even though it is found that the reduced model has a slightly higher burning rate (Fig. 4), counter intuitively it predicts a slightly

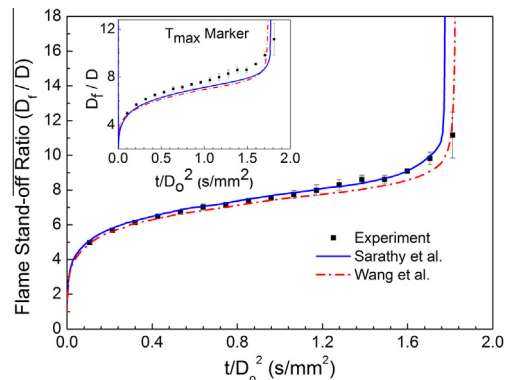


Fig. 6. Comparison between measured and predicted FSR for *n*-butanol droplet ($D_0 = 0.56$ mm, 1 atm, 21% O_2 /balance N_2 . HRR_{max} marker: central figure; T_{max} marker: inset figure.

smaller FSR indicating the flame to be located closer to the droplet. It is due to this fact that even with slightly lower flame temperature the reduced model predicts a higher burning rate.

To further elucidate the flame structure and kinetic effects of n -butanol, computations were performed for a broad range of ambient oxygen concentrations ($0.08 \leq X_{O_2} \leq 0.21$). Figure 7 presents predicted K_{avg} , T_{avg} , FSR_{avg} and the normalized extinction diameter (D_{ext}/D_o) as a function of oxygen concentration, X_{O_2} . The numerical data are obtained by time averaging the predicted values over the range $0.10 < t_b < 0.95$. In general these average quantities provide insight into the quasi-steady combustion characteristics. As the figure illustrates, increasing X_{O_2} increases the burning rate by increasing the flame temperature. Both K_{avg} and T_{avg} show an almost linear variation as a function of X_{O_2} . By contrast, the FSR_{avg} decreases with increasing X_{O_2} , as stoichiometric conditions are achieved nearer the droplet surface.

As the limiting oxygen index (LOI) is approached (i.e. decrease in O_2), a sharp decrease in the FSR_{avg} is observed. This decrease is due to an inability to achieve quasi-steady burning conditions. Based on the variation of the FSR_{avg} the LOI for these sub-millimeter sized n -butanol droplets is found to be 0.10. Extinction starts occurring at $X_{O_2} = 0.16$ with sharp increases in extinction diameter as LOI's are approached.

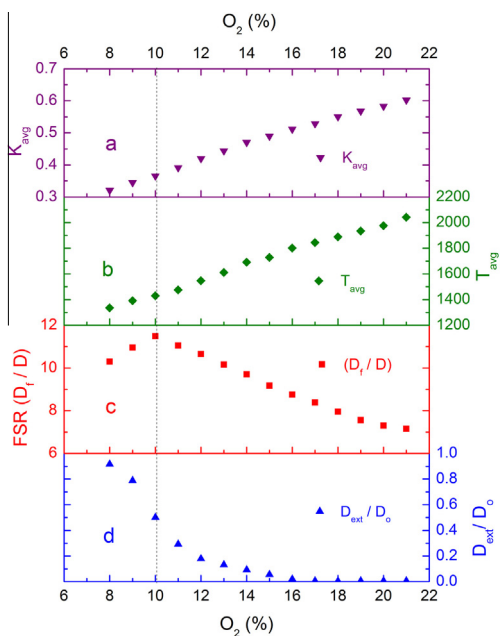


Fig. 7. Predicted (a) K_{avg} , (b) T_{avg} (c) FSR_{avg} and (d) normalized extinction diameter (D_{ext}/D_o) as a function of X_{O_2} for n -butanol droplet using detailed kinetics [23] ($D_o = 0.56$ mm, 1 atm). The dashed line marks the location of LOI.

Unlike other C_1 – C_3 alcohols (i.e. methanol, ethanol and propanol) n -butanol does not absorb water; therefore flame extinction in these small sized droplets is not due to water dissolution rather kinetic effects.

The evolutions of peak mass fraction (PMFs) for some selected species are presented in Figs. 8 and 9 for $X_{O_2} = 13\%$ and 21% respectively. In this high temperature droplet combustion, the n -butanol is predominantly decomposed in the burning process by H abstraction/alkyl/radical beta scission reactions [23]. Hydrogen atom is the principle abstractor, consuming majority of the fuel. Among the intermediates, C_2H_4 is the most prominent species for both the cases, which is followed by C_2H_2 and C_3H_6 . Ethylene in n -butanol combustion has been reported either through H-abstraction in α -position, producing ethyl radicals, which subsequently forms C_2H_4 through β -scission [10,13] or via ω -Hydrogen abstraction producing C_2H_4 as a direct β -scission product ($nC_4H_9OH \rightarrow C_4H_8OH\cdot \rightarrow C_2H_4 + pC_2H_4OH$) [14]. The large amounts of C_2H_4 also promote the formation of vinyl radicals (C_2H_3). The consumption pathways of C_2H_3 result in the formation of C_2H_2 ($C_2H_3 + H \rightarrow C_2H_2 + H_2$). However, in comparison, C_2H_6 and C_3H_8 are found to be lower by an order of magnitude, which is qualitatively in congruence with ref [34]. Recombination of methyl and ethyl radicals, along with H-abstraction from formaldehyde by n -propyl radicals contribute to C_3H_8 formation

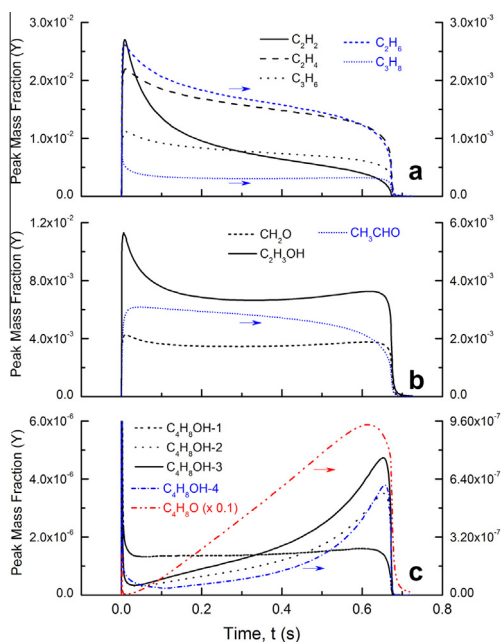


Fig. 8. Predicted temporal evolution of peak mass fraction of selective species for n -butanol droplet combustion ($D_o = 0.56$ mm, 13% O_2 /balance N_2 , 1 atm).

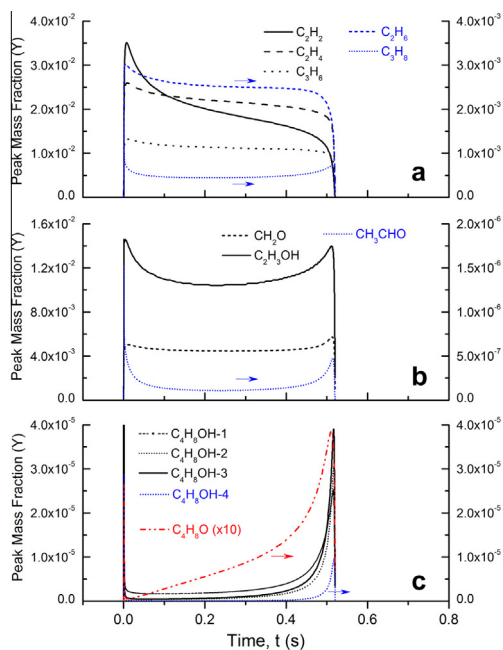


Fig. 9. Predicted temporal evolution of peak mass fraction of selective species for *n*-butanol droplet combustion ($D_0 = 0.56$ mm, 21% O_2 /balance N_2 , 1 atm).

[32]. All these species are formed in the fuel rich side of the diffusion flame structure [20]. At lower Damköhler numbers (i.e. $X_{O_2} = 13\%$), all the smaller C-H species PMF profiles remains nearly same except C_2H_2 , which reduces by a factor ~ 2.2 indicating that *n*-butanol is less susceptible to soot formation even in lower O_2 environments. On the other hand, for C_3H_6 , the significant formation channel are: (i) $C_4H_8OH-3 \rightarrow C_3H_6 + CH_2OH$ where C_4H_8OH-3 is directly formed from parent fuel via H abstraction [32] and (ii) $C_4H_8(1\text{-Butene}) + H = C_3H_6 + CH_3$ and $n\text{-}C_3H_7 = C_3H_6 + H$ [35].

Ethanol and ethanal are two important isomers of C_2H_4O where ethanal is tautomerized from ethanol. In contrast to experimental evidence [36] and similar to kinetic modeling observations reported in ref [23], peak concentration of ethanol (C_2H_3OH) was found to be consistently higher than ethanal throughout the combustion for both the O_2 cases, which implies a lack of characterization of ethanol consumption and/or overestimation of overall flux balance of H-atom abstraction to α -carbon (Figs. 8 and 9). C_2H_3OH is formed via two major channels $C_4H_8OH-1 \rightarrow C_2H_3OH + C_2H_5$ and $pC_2H_4OH \rightarrow C_2H_3OH + H$, where C_4H_8OH-1 is formed by H abstraction of *n*-butanol and pC_2H_4OH is majorly formed by the decomposition of C_4H_8OH-4 . And, the predicted peak mass fraction of CH_3CHO is seen to be significantly lower for $X_{O_2} = 21\%$.

However, for $X_{O_2} = 13\%$, the concentration of ethanol is reduced by $\sim 40\%$ probably because of slower burning rate at $X_{O_2} = 13\%$ condition decreases the fuel evaporation rate, which lead to a decrease in C_4H_8OH concentration. Formaldehyde is believed to form primarily through two main pathways: (i) ‘H-abstraction’ following β -scission of C_4H_9O (directed from fuel) [23,34]; (ii) from *n*-butoxy radical [14]. As the droplet shrinks (for a given X_{O_2}) or with the change in O_2 concentration, the CH_2O profiles remain unaltered suggesting lower probability of first type of reaction pathway for spherically symmetric droplet combustion environment.

C_4H_8OH is formed by H-abstraction of parent fuel molecule by H-atom and methyl radical, which subsequently decomposes to C_4H_8O and other species [32]. It was reported that β -scission of 1-hydroxybutyl radical is the exclusive route to butanal [13,14], while Sarathy et al. [23] advocate β -scission of *n*-butoxy radical as the important route. Harper et al. [32] found that assisted elimination reaction of 1-hydroxybutyl by atomic O is important for butanal formation. Alternately, Sarathy et al. also proposed butanal/butanone production via $C_4H_8OH-1 + O_2 = n\text{-}C_3H_7CHO + HO_2$, at relatively low temperature conditions and higher O_2 concentration [36]. Comparing Figs. 8c and 9c it can be seen that the peak C_4H_8O (butanal) increases by a factor of ~ 2.4 ($\sim 9.6/4.0$) when the droplet burns in lower O_2 condition which is a consequence of the low flame temperature. The peak butanal concentration is also observed to increase steadily and almost linearly during the entire burn process at low oxygen concentration. These trends of butanal species concentration at low Damköhler numbers are similar to that observed in opposed flow diffusion flame configuration.

5. Concluding remarks

Spherically symmetric, isolated *n*-butanol droplet combustion has been studied experimentally and numerically. The *n*-butanol data were compared against predictions from a comprehensive numerical model of droplet combustion, employing both a detailed and reduced kinetic model. The experiments showed no presence of a soot shell during the combustion process and droplets were observed to burn to completion unlike other smaller C_1 – C_3 alcohols. Predictions from the numerical model were in favorable agreement with the experimental measurements for both models showing complete combustion and no extinction. Additionally it was found that the detailed and reduced kinetic models had minimal differences among them; $\sim 3\%$ variation in the average burning rate and ~ 40 K difference in the peak temperature.

To further elucidate the flame structure and kinetic effects, simulations were conducted over a broad range of oxygen concentration to identify the limiting oxygen index and variation of the droplet extinction diameter. The model predicted that for sub-millimeter sized *n*-butanol droplets the limiting oxygen index is as low as 10% suggesting that flame extinction for *n*-butanol is unlikely in practical applications.

Analysis of the kinetics within the droplet flame structure showed that *n*-butanol produces significant amounts of C₂, C₃ stable intermediates as well as comparable amounts of formaldehyde acetaldehyde and vinyl alcohol. The peak acetylene concentration was higher only during the very early stages of the burn and drastically reduced as quasi-steady burning was achieved – thereby reducing the possibility of any soot or soot shell structure formation. For cases where extinction of the flame occurred steadily increasing buildup of the large fuel fragments (i.e. C₄H₈OH-3, C₄H₈OH-2 and C₄H₈OH-4) was observed.

Acknowledgements

This work was supported by the National Aeronautics and Space Administration through grant numbers NNX09AW 19A (for FLD), NNX08AI51G (for YCL and CTA) and the University of South Carolina Startup Fund (for FEA and TIF). Special thanks to Mr. Michael Hicks, Dr. Daniel Dietrich of NASA for their interest and assistance throughout the course of this investigation. The authors are also thankful to Prof. Rolf Reitz of University of Wisconsin-Madison for sharing their kinetic database.

Appendix A. Supplementary data

Supplementary data associated with this article can be found, in the online version, at <http://dx.doi.org/10.1016/j.proci.2014.06.043>.

References

- [1] B.G. Harvey, H.A. Meylemans, *J. Chem. Technol. Biotechnol.* 86 (2011) 2–9.
- [2] C. Jin, M. Yao, H. Liu, C.F. Lee, J. Jing, *Renewable Sustainable Energy Rev.* 15 (2011) 4080–4106.
- [3] C.K. Law, *AIAA J.* 50 (2012) 19–36.
- [4] D. Healy, H.J. Curran, J.M. Simmie, et al., *Combust. Flame* 155 (2008) 441–448.
- [5] T. Lu, C. Law, *Combust. Flame* 146 (2006) 472–483.
- [6] E.R. Ritter, J.W. Bozzelli, *Int. J. Chem. Kinet.* 23 (1991) 767–778.
- [7] X. Gu, Z. Huang, Q. Li, C. Tang, *Energy Fuels* 23 (2009) 4900–4907.
- [8] P. Dagaut, C. Togbé, *Fuel* 87 (2008) 3313–3321.
- [9] P. Dagaut, C. Togbé, *Energy Fuels* 23 (2009) 3527–3535.
- [10] P. Dagaut, S.M. Sarathy, M.J. Thomson, *Proc. Combust. Inst.* 32 (2009) 229–237.
- [11] S.M. Sarathy, M.J. Thomson, C. Togbé, P. Dagaut, F. Halter, C. Mounaim-Rousselle, *Combust. Flame* 156 (2009) 852–864.
- [12] P. Dagaut, C. Togbé, *Fuel* 89 (2010) 280–286.
- [13] J.T. Moss, A.M. Berkowitz, M.A. Oehlschlaeger, J. Biet, V. Warth, P. Glaude, F. Battin-Leclerc, *J. Phys. Chem. A* 112 (2008) 10843–10855.
- [14] G. Black, H.J. Curran, S. Pichon, J.M. Simmie, V. Zhukov, *Combust. Flame* 157 (2010) 363–373.
- [15] S.M. Sarathy, M.J. Thomson, W.J. Pitz, T. Lu, *Proc. Combust. Inst.* 33 (2011) 399–405.
- [16] H. Wang, R.D. Reitz, M. Yao, B. Yang, Q. Jiao, L. Qiu, *Combust. Flame* 160 (2013) 504–519.
- [17] A. Amsden, LA-UR-99-915, 1999.
- [18] W.A. Sirignano, *Fluid dynamics and transport of droplets and sprays*, U.P., Cambridge, 1999, pp. 10–21.
- [19] A. Cuoci, M. Mehl, G. Buzzi-Ferraris, T. Faravelli, D. Manca, E. Ranzi, *Combust. Flame* 243 (2005) 211–226.
- [20] T. Farouk, F.L. Dryer, *Combust. Theory Model.* 15 (2011) 487–515.
- [21] T. Farouk, F.L. Dryer, *Combust. Flame* 159 (2012) 200–209.
- [22] T. Farouk, Y.C. Liu, A.J. Savas, C.T. Avedisian, F.L. Dryer, *Proc. Combust. Inst.* 34 (2013) 1609–1616.
- [23] S.M. Sarathy, S. Vranckx, K. Yasunaga, M. Mehl, P. Oswald, W. Metcalfe, C. Westbrook, W. Pitz, K. Kohse-Hoinghaus, R. Fernandes, H. Curran, *Combust. Flame* 159 (2012) 2028–2055.
- [24] S. Nakaya, K. Fujishima, M. Tsue, M. Kono, D. Segawa, *Proc. Combust. Inst.* 34 (2013) 1601–1608.
- [25] Y.C. Liu, C.T. Avedisian, *Combust. Flame* 159 (2012) 770–783.
- [26] C.T. Avedisian, J.C. Yang, C.H. Wang, *Proc. R. Soc. Lond. Ser. A Math. Phys. Eng. Sci.* 420 (1988) 183–200.
- [27] C.T. Avedisian, B.J. Callahan, *Proc. Combust. Inst.* 28 (2000) 991–997.
- [28] Y.C. Liu, *Droplet combustion of surrogate and real fuel systems in a low convection condition ground based and space based experiments*, Ph.D. thesis, Cornell University, Ithaca, NY 14853, USA, 2013.
- [29] C. Dembia, Y.C. Liu, C.T. Avedisian, *Image Anal. Stereology* 31 (2012) 137–148.
- [30] T.E. Daubert, R.P. Danner, *Physical and Thermodynamic Properties of Pure Chemicals: Data Compilation*, Hemisphere Publishing, New York, 1989.
- [31] S. Vranckx, K. Heufer, C. Lee, H. Olivier, L. Schill, W.A. Kopp, K. Leonhard, C.A. Taatjes, R.X. Fernandes, *Combust. Flame* 158 (2011) 1444–1455.
- [32] M.R. Harper, K.M. Van Gem, S.P. Ply, G.B. Martin, W.H. Green, *Combust. Flame* 158 (2011) 16–41.
- [33] S.R. Turns, *An Introduction to Combustion, 2nd edit.*, McGraw-Hill, New York, 2000, p. 376–391.
- [34] P. Oßwald, H. Güldenber, K. Kohse-Hoinghaus, B. Yang, T. Yuan, F. Qi, *Combust. flame* 158 (2011) 2–15.
- [35] J. Cai, L. Zhang, F. Zhang, Z. Wang, Z. Cheng, W. Yuan, F. Qi, *Energy Fuels* 26 (2012) 5550–5568.
- [36] N. Hansen, M.R. Harper, W.H. Green, *Phys. Chem. Chem. Phys.* (2011) 20262–20274.